Jinst

Published by IOP Publishing for Sissa Medialab

Received: *February 21, 2023*
Accepted: *April 10, 2023*
Published: *June 26, 2023*

Track reconstruction and analysis of particle interactions in short bent crystals

R. Rossi,[a,b,*] **L.S. Esposito,**[a] **M. Pesaresi,**[b] **G. Hall**[b] **and W. Scandale**[b,c]

[a] *European Organization for Nuclear Research, CERN, 1 Esplanade des Particules, Meyrin, Switzerland*
[b] *Blackett Laboratory, Imperial College, Prince Consort Road, London SW7 2AZ, U.K.*
[c] *Sezione di Roma 1, INFN, Piazzale Aldo Moro 2, 00185 Rome, Italy*

E-mail: Roberto.Rossi@cern.ch

Abstract: Measurements of the interaction of positively charged particles with bent crystals were obtained by developing a new and consolidated analysis method, for the use of UA9 collaboration. The method was deployed to characterize crystals with a length of a few mm along the beam direction and a bending angle in the order of 10 µrad to 100 µrad, typically exploited in the CERN accelerators. To assess their properties and quality, the crystals have been investigated in the Super Proton Synchrotron North Area with a beam of mixed hadrons at 180 GeV. The UA9 telescopic tracker has been used to collect the data. Some of them are used in the present study to describe and validate the applied data-analysis methodology.

Keywords: Analysis and statistical methods; Data processing methods; Particle tracking detectors

*Corresponding author.

https://doi.org/10.1088/1748-0221/18/06/P06027

2023 JINST 18 P06027

Contents

2023 JINST 18 P06027

1 Introduction

Positively charged particles, penetrating through a mono-crystal, may be captured in channeling states into the electrostatic potential of the regularly distributed nuclei, showing reduced probability of multiple Coulomb scattering (MCS), nuclear interactions (INI) and ionization loss. The necessary condition for channeling is a low value of the impact angle θ at the crystal entrance relative to the crystalline planes direction [1]. The critical impact angle for particle confinement in the planar potential well $U_{\max}$ between two crystalline planes is $\theta_c = \sqrt{2U_{\max}/pv}$, where p and v are the particle momentum and velocity respectively. For Si (110) planes, $U_{\max} \approx 20\,\text{eV}$.

In a bent crystal, particles may be channeled if the bending radius R is larger than the critical value $R_c = pv/eE_c$, where E_c is the electric field intensity at the boundary of the stable trajectory region [2]. For straight Si (110) planes, $E_c \approx 6\,\text{GeV cm}^{-1}$. As R decreases, the inter-planar potential well becomes increasingly asymmetric and ineffective and the critical angle is reduced [3]. Bent

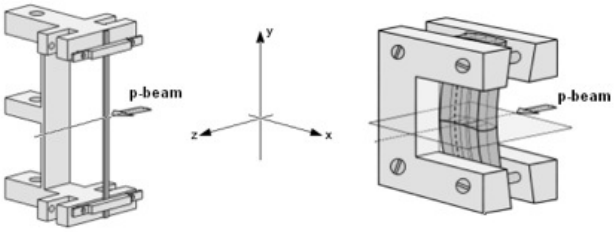

Figure 1. Schematic view of short crystals. Left: strip crystal using anticlastic bending. Right: crystal slab using quasimosaic bending.

2023 JINST 18 P06027

crystals can deflect incoming particles, through channelling (CH) or volume reflection (VR) [4] mechanisms. In CH, particles are deflected by $\theta_b = l/R$, the bending angle of the crystalline planes, where l is the crystal length. However, the CH efficiency P_{CH} decreases with R. The record value $P_{CH} = 0.75$ for 400 GeV protons channeled by a 1.94 mm long Si(110) crystal, with $\theta_b = 50\,\mu$rad, $R = 38$ m and $\theta_c \approx 10\,\mu$rad, is reported in [5]. Concurrent processes for CH are dechanneling induced by MCS with the electrons and the nuclei of the crystal array, INI occurring due to nuclear interactions and VR due to dechanneling followed by a reflection in the crystal volume. Interactions with the defects of the crystalline structure increase the dechanneling probability. In VR, particles with θ slightly larger than θ_c reflect out of the curvature when they are nearly parallel to the planes, at the tangent point of the incoming trajectory with the arc of the crystalline planes. The VR deflecting angle θ_{VR} is proportional to θ_c. For Si(110), $\theta_{VR} \approx 1.3\theta_c$, while, for $R \approx 10R_c$, the VR efficiency P_{VR} can exceed 95% [6]. P_{VR} decreases as R increases, because the effective potential becomes more and more symmetric [7]. For 400 GeV protons on Si(110), with $R \approx 18$ m, $\theta_{VR} \approx 13\,\mu$rad [8].

The use of bent crystals for beam manipulations in particle accelerators or in external beam-lines is an old concept still under scrutiny [9]. In the last three decades, the knowledge on the features of crystal-particle interaction has been continuously growing on the basis of a large number of experimental findings. In all cases, the results of measurements have been found in agreement with, and sometimes have been anticipated by, numerical models and simulations. Short crystals, optically or chemically polished, with constant curvature obtained through anticlastic or quasi-mosaic elastic reaction [10, 11], schematically shown in figure 1, have demonstrated a large exploitation potential in particle accelerators. The UA9 Collaboration has extensively tested a large number of them in the extracted beam lines of the SPS North Area with beams of various species, such as protons, electrons and heavy-ions, in the range up to a few hundred GeV energy. The work-horse instrument exploited was a two arm telescope made of five silicon-strip detectors, providing a very precise angular reconstruction of the particle trajectories [12–14]. The experimental results are discussed in detail in [15].

In this paper we illustrate the data analysis implemented in UA9 to provide information on the kinematics and the cross-section of the high-energy particle interactions occurring during the crystal traversal. Its application to the crystals required for the CERN accelerator complex shows in detail useful examples of the methods.

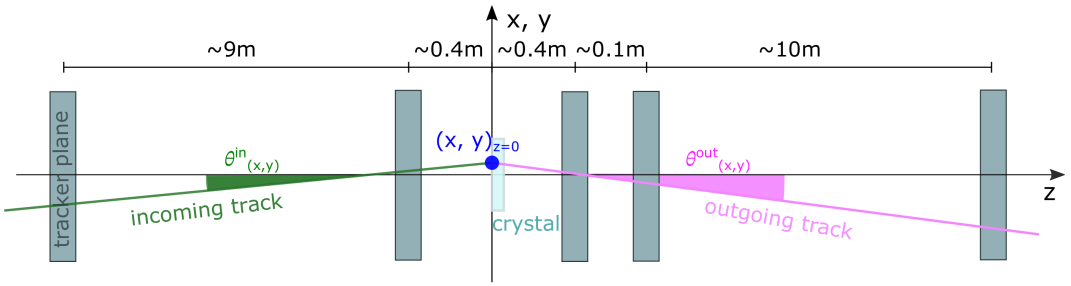

Figure 2. Tracker telescope layout. The crystal (light blue box) is placed at the center of the reference system. Five silicon tracker planes (gray boxes) compose the two arm telescope. Distances between consecutive elements are shown. Incoming (green line and angle) and outgoing (magenta line and angle) tracks are shown. The z-vertex interaction point is highlighted.

2 Experimental layout

The primary beam, made of protons or heavy-ions, extracted from the CERN Super Proton Synchrotron (SPS) toward the North Area is routinely exploited in several experimental areas. One of them, called H8 line, can be optimized to achieve a micro-beam with a few tenths of µrad RMS-divergence and a few mm spatial RMS-size, suitable for investigating crystal-particle interactions and characterising crystal features. In general, primary beams have an energy of 400 GeV per charge, while secondary beams of hadrons or muons have 180 GeV energy.

The most upstream area of the H8 beam line houses the UA9 setup, schematically shown in figure 2. The reference frame $O(x, y, z)$ is the same of figure 2, with its origin at the position of the crystal entry face, with the xy-plane orthogonal to the bent crystalline planes and with the z-axis parallel to the beam direction. The tracking detector telescope about 20 m long is used to reconstruct the trajectories of the incoming particles interacting with a bent crystal mounted on a goniometer. In channeling orientation the crystal will deflect the incoming particles along the horizontal plane by its bending angle θ_b. The goniometer is a high precision multi-stage actuator, made of a linear stage that allows translating the crystal in and out of the beam line along the x-axis, and a rotational stage to modify the horizontal orientation of the crystal relative to the beam line. The tracker is composed of five stations (or planes) each hosting a pair of silicon strip sensors, mounted perpendicular to each other to resolve the particle hit in both the horizontal and vertical directions. The incoming arm of the telescope is composed of two tracker stations, while the outgoing one consists of three stations. In its standard configuration, the incoming and outgoing arms are arranged to have a length of about 10 m on either side of the crystal. Each of the sensors has an active width of 98 mm and there are 639 strips on a 60 µm pitch so the effective aperture for xy-plane measurements in each pair of stations is 3.8 cm × 3.8 cm. The maximum deflection measurable is ≈2.5–3.5 mrad, depending on the accuracy of the transverse positioning of the stations to the beam line. Larger deflection measurements require changing the shape of the telescope outgoing arm [16]. To reduce the interaction of beam particles with air, the tracker stations are installed where segments of vacuum beam pipes are removed. The longest vacuum pipe sections are in between the first and second plane and between the fourth and fifth plane.

2023 JINST 18 P06027

3 Data acquisition

In each run, various sequences of data are acquired. After the detector installation, the geometry of the telescope is accurately recorded. Then, the beam is injected with the crystal in retracted position, to evaluate its shape and divergence and the telescope angular accuracy. Further steps consist in inserting the crystal and optimising its overlap with the beam, in performing angular scans to identify the channeling orientation and in acquiring large set of data in an angular range where coherent crystal-particle interactions happen. Finally the parameters of each particle track are computed and stored. Details are discussed in the following sub-sections.

3.1 Preparatory phase

A preparatory phase is required before each experimental period, to install the setup in its optimal configuration, check the characteristics of the incoming beam and evaluate the detector performance.

Each crystal, mounted in its bending support, is attached to the goniometer and aligned to the beam direction using external referential markers, a laser source and a reflector. This minimises the time to bring the crystal orientation into the angular range of interest by a lengthy angular scan procedure. The optical alignment procedure has been optimised to the point that crystals could be quickly oriented within few hundred µrad from perfect channeling orientation.

The beam exploitation starts with the so-called "alignment run", performed with crystal in a retracted position from the beam line. The goal is to determine the actual values of the transverse beam shape and divergence, the mutual alignment of the planes and the angular resolution of the tracker. Such values will later be used to calibrate the track reconstruction algorithm during the successive crystal characterisation.

3.2 Finding the channeling orientation

During crystal run, the Data Acquisition User Interface (DAQ) of the tracker telescope acquires the tracks and synchronises them to the actual crystal position and orientation. The DAQ includes the online processing of a small subset of the tracks. The result is presented in real time, in a continuously refreshed incremental plot, useful to control the progression of the run. The number of tracks in the subset is selected by the user, depending on the desired refresh rate.

The online processing helps in positioning the crystal, generally thinner that the beam spot, in the best position to maximise the interaction rate with the beam. Moreover, by changing the crystal orientation, the online processing allows to identify the channeling orientation and the angular range for more accurate investigation.

3.3 Crystal investigation runs

The detailed overview of the crystal-particle interactions as a function of the impact angle θ is obtained by rotating the goniometer in fine steps over an angular range slightly larger than θ_b, around the optimal orientation for channeling (angular scan). For each angular orientation, 1×10^6 to 2×10^6 events are collected, limited by the run duration.

In high-statistic runs, large set of data are recorded with the crystal at fixed orientation, for an accurate evaluation of the probability of channeling, amorphous or VR process. Each data-set typically contains 16×10^6 events, limited by the available DAQ memory.

2023 JINST 18 P06027

3.4 Reconstruction of the particle kinematics

The online data reconstruction during the test beam is limited because the computer resources and algorithm should simultaneously provide the track reconstruction and storage and the online analysis. The full data reconstruction is thus performed offline at the end of each experimental period, taking into account several parameters, as described in detail in [14].

The data of the alignment run, recorded with the crystal out of the beam path, represent slightly perturbed straight tracks. They could be used to evaluate the relative alignment of stations along the tracker and to re-calibrate the tracking reference system. They also provide a refreshed estimate of the tracker angular resolution, defined as the standard deviation of the deflection detected in the two telescope arms, that depends on MCS induced by the total material budget (tracker stations, pipe windows and air), as well as the micro-strip dimensions and separations.

During crystal measurements, for each event, the 2D hit points of each station are identified. Events with multiple hits in the incoming arm are discarded, while those in the outgoing arm are flagged for special analysis. The tracks, reconstructed from the recorded hits on each plane, are compared to a χ^2 criterion. The imposed fit constraint is that outgoing and incoming tracks have a point-like interaction vertex at the crystal entrance position (i.e. $z = 0$ in the reference system of the telescope), taking into account the multiple scattering error correlation. Six parameters are extracted from the fit: the horizontal and vertical angular projections of the incoming trajectory (θ_x^{in}, θ_y^{in}) and of outgoing trajectory (θ_x^{out}, θ_y^{out}), and the transverse coordinates of the interaction vertex $(x,\ y)_{z=0}$. They are used as input for the crystal characterisation.

Crystals used in high-energy accelerators, such as the CERN LHC and SPS, are a few mm long, hence, the assumption of a point-like interaction vertex is sufficiently accurate. This method of reconstructing and selecting the particle trajectories was deployed since 2012. More than 300 crystals for various applications were tested in H8 [16–18], demonstrating reliability of tracker performance with different hadron and ion beams.

4 Data analysis

The data analysis is mainly focused on the reconstruction of crystal-particle interactions as a function of the horizontal impact angle. The main observables are the probability of channeling and VR process, the deflection angle and the crystal torsion. Tracker resolution, beam size and MCS deflection are provided as well.

Different criteria are applied to extract information on the beam shape and telescope performance from the alignment runs, and on the crystal-particle interactions from the high-statistics measurements.

Details are discussed in the following paragraphs.

4.1 Alignment runs

The geometrical configuration of the UA9 setup and the parameters of the incoming beam may differ from one run to another, because of the multi-user operation of the H8 beam line that implies to install and remove the UA9 setup in each experimental session and to adapt the beam specification to different needs. The alignment runs are specifically devoted to calibrate the reconstruction algorithm at the beginning of each UA9 run.

2023 JINST 18 P06027

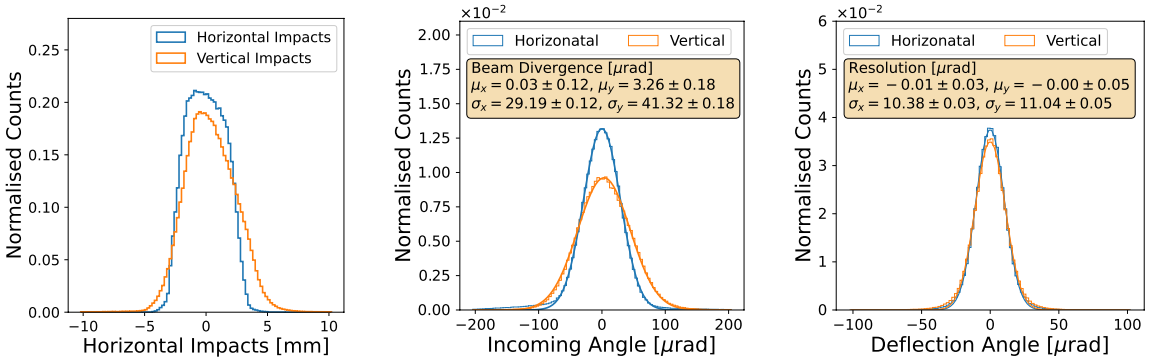

(a) Horizontal (blue) and Vertical (orange) impact distributions.

(b) Horizontal (blue) and Vertical (orange) impact angle distributions.

(c) Horizontal (blue) and Vertical (orange) tracker resolution distributions.

Figure 3. Beam parameters (3(a) and 3(b)) and tracker resolution (3(c)) measured during an UA9 alignment run.

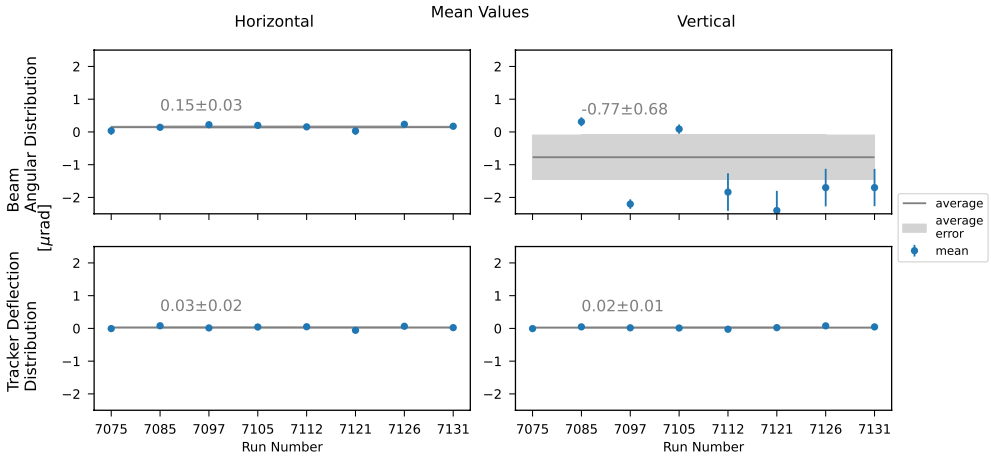

Figure 4. Stability of Mean Values with Run Number for impact beam angular (top row) and tracker measured deflection for straight particles (bottom row). Horizontal and vertical projections are presented on the left and right columns respectively. The fluctuations observed in the vertical angular distribution were addressed by the beam operators after the run 7105.

In figure 3, the information extracted from a typical alignment run, with the crystal out of the beam, is reported. The plot in 3(a) gives the horizontal and vertical spatial beam distributions, both rather far from Gaussian shape. The plot in 3(b) shows the horizontal and vertical beam divergences, both with an almost Gaussian shape. Finally, the plot in 3(c) illustrates the horizontal and vertical angular resolutions of the telescope, defined as the standard deviation of the deflection for straight tracks. Because of the MCS, each track should have slightly different directions in the incoming and in the outgoing telescope arms. The straight track deflection is defined as the difference of the two angular directions. The deflection distribution is Gaussian and its standard deviation is used to define the overall telescope resolution.

Information on the incoming beam gathered though the alignment run is sometimes provided to the North Area experts, to prepare and verify special setups of the H8 beam line.

2023 JINST 18 P06027

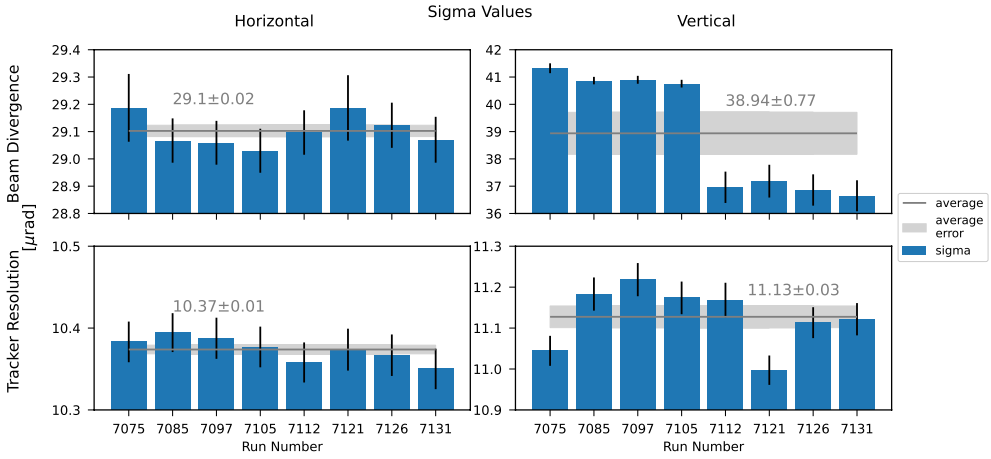

Figure 5. Beam divergence (top) and tracker resolution (bottom) measured during an UA9 alignment run. As observed in figure 4 fluctuations observed in the vertical angular distribution were addressed by the beam operators after the run 7105.

The alignment data collected at the beginning of a high-statistics run generally provide adequate information for the algorithm calibration over an entire High-Statistics run. In figure 4, alignment data repeatedly collected over two weeks are shown. The mean values of the beam impact angle (top) and the track deflection at the interaction vertex due to MCS (bottom) are shown for the horizontal (left) and the vertical (right) planes. In figure 5, the average beam divergence and the average tracker resolution are given. They illustrate the variations of the alignment parameters, indeed rather weak, that could affect high-statistics runs lasting a couple of weeks.

4.2 High-statistics runs in channeling orientation runs

Crystals to be used for beam manipulations in circular accelerators, require a preliminary validation of their performance with an extracted beam. In particular, the probability of channeling and VR process give information about the structure of the crystalline lattice that cannot be measured by optical inspection. The data handling procedures dedicated to UA9 have been developed, deployed and continuously upgraded since 2010. For the correct evaluation of the crystal-particle interaction rates as a function of the track impact angle, macroscopic features should be compensated; these features are dependant on the elastic response of the whole crystal to the deformation applied and thus are independent of the crystalline lattice. A geometrical cut is applied to exclude from the analysis all the tracks with the interaction vertex $(x,\ y)_{z=0}$ out of the crystal entry face. The torsion of strip crystals and the saddle deformation of Quasi-Mosaic (QM) crystals [11] is measured and numerically compensated to simplify the treatment of the track dependence on the vertical impact parameter. The average offset of the beam orientation relative to the crystalline plane is measured and taken into account in evaluating the impact angle of each track. Finally, the amorphous orientation mean deflection is measured and used to adjust the overall deflection distribution. This value should be as close as possible to zero, to ensure the numerical compensation of any possible misalignment in the absolute reference frame.

2023 JINST 18 P06027

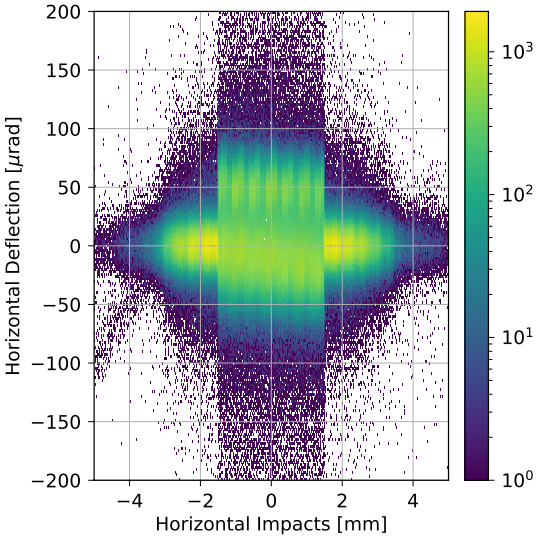

Figure 6. Density plot for Horizontal Deflection vs Impacts. The effect of the crystal in the beam is clearly highlighted by the changes of the deflection distribution.

The numerical correction of the particle trajectories provides a homogeneous data-set to estimate the dependence of the horizontal deflection on the impact angle, mitigating the loss in statistics, otherwise unavoidable. Such a high-statistics data-set is used to evaluate details of the amorphous, volume reflection and channeling behaviour. The data processing also provides accurate information on the bending angle and the torsion of the crystalline planes around the vertical axis.

4.2.1 Geometrical cuts

Crystals used in the CERN accelerator complex are usually made with an impact face about 2 mm to 3 mm wide and 40 mm to 50 mm high. The vertical dimension is generally larger than the H8 beam spatial distribution, while the horizontal dimension is smaller, as shown in the density plot of figure 6. A geometrical cut is introduced to select tracks hitting the crystal face. The selection algorithm is different for the horizontal and the vertical planes, see figure 7.

The horizontal crystal extremities are identified through the analysis of the horizontal track deflection as a function of impact parameter. The horizontal axis is split in bins of 40 μm width. Tracks with impact positions in the same bin form a data subset. In each subset i, the standard deviation of the track deflections $\sigma_i(\Delta\theta_x)$ and the 95 % confidence interval $\delta\sigma_i(\Delta\theta_x)$ that contains the "true" value of the standard deviation are computed. The plot of these values as a function of the bin position, allows to identify the contour of the crystal in the tracker reference frame. The selected tracks are those with an RMS deflection larger than a threshold, shown by a red line in the left side plot of figure 7(a). The threshold value is empirically given by the expression: $\max \sigma_i(\Delta\theta_x) - \Delta$, with $\Delta = \sigma(\sigma_i(\Delta\theta_x))$.

In the vertical plane, the normalized counting rate as a function of the vertical impact distribution is considered. Although such distribution is not Gaussian, as shown in the example of figure 7(b), the track selection is restricted to events whose rate exceeds the maximum value minus one standard deviation.

Only tracks that passes both tests are considered.

2023 JINST 18 P06027

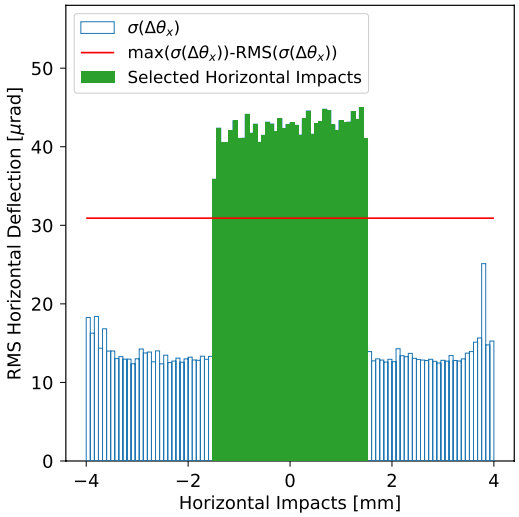

(a) RMS values for horizontal deflection binned by horizontal impact. The solid red line shows the selection threshold, the solid green bars shows the horizontal impacts values within the selection.

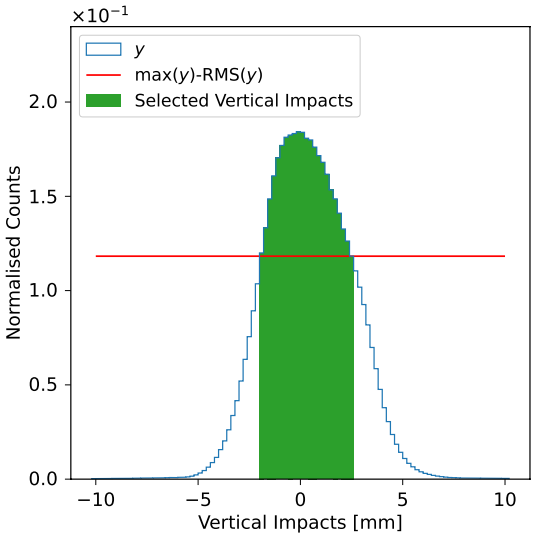

(b) Vertical impacts distribution. The solid red line shows the selection threshold, the solid green bars shows the vertical impacts values within the selection.

Figure 7. Horizontal (a) and the vertical (b) track selections.

4.2.2 Data correction

The torque induced by the mounting of a strip crystal on its bending device may gives rise to a twist around the vertical axis in its shape, which results in torsion. Crystal torsion induces a shift of the particle deflection as a function of the vertical impact point. Moreover, the average value of the deflection distribution with the crystal in amorphous orientation imposes a global shift of the deflection distribution in all the possible crystal orientations. Corrections are required to make the data coherent to each other, thus to enlarge the track statistics. They consist in applying the linear transformations:

$$\theta^{\text{in}}_{\text{corr}} = \theta^{\text{in}}_{\text{x}} + (t \times y - o), \tag{4.1}$$

$$\Delta\theta_{\text{corr}} = \Delta\theta_{\text{x}} - \theta_{\text{AM}}, \tag{4.2}$$

where t is the torsion of the crystal, expressed in $\mu\text{rad}\,\text{mm}^{-1}$, y is the vertical impact point of the tracks, o is the offset, i.e. the angle between the beam main direction and the crystalline plane orientation, and θ_{AM} is the average value of the amorphous distribution. The example in figure 8 shows how the equations (4.1) and (4.2) could modify the density plot correlating deflections and impact angles. The reference frame in figure 8 is the same of the one in figure 2.

Uncorrected data are used to evaluate the parameters t, o and θ_{AM} as described in paragraphs 4.2.3, 4.2.4 and 4.2.5.

2023 JINST 18 P06027

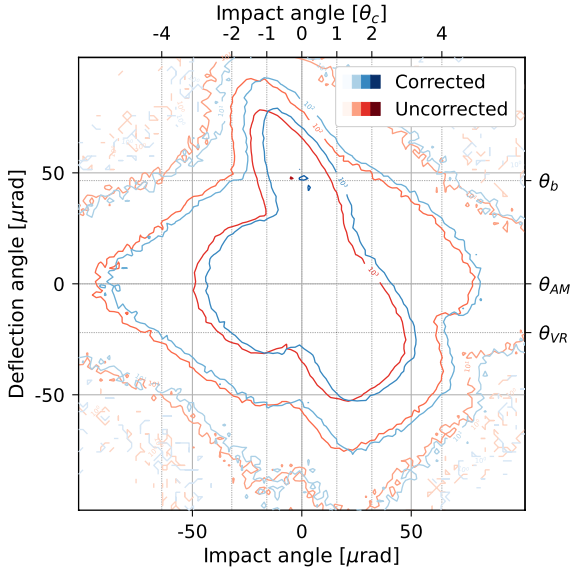

Figure 8. Density plot of the deflection versus the impact angle: uncorrected (in red) and corrected (in blue) contour lines are shown.

4.2.3 Torsion measurement

The torsion t might change the relative direction of the crystalline planes as a function of the vertical impact parameter. Its numerical compensation, described in paragraph 4.2.2, prevent loss of statistic for the channeling efficiency evaluation.

A set of data collected with the crystal in channeling orientation can provide the torsion measurement, as shown in the example of figure 9. The vertical axis is segmented in bins of 0.2 mm height and the tracks are separated in subsets with the vertical impact parameter in the same bin (see top-left plot). For each subset, the mean deflection angle is evaluated by the Gaussian fit of deflection distribution (see bottom-left plot). The crystal torsion value corresponds to the coefficient of the linear correlation between the mean deflection angle and the vertical impact parameter (see right plot).

4.2.4 Offset of the impact angle distribution

The mean value of the beam divergence might be different from the crystalline plane direction. The offset should be numerically corrected through the equation (4.1), to avoid misinterpretations of the crystal parameters.

The offset value is found by identifying the channeling spot in the density distribution of the track impact angles, as shown in figure 10. The impact angle is segmented in slices of 2 µrad (left plot). The number of tracks in each slice allows to build the impact angle distribution (right plot). The blue dots represent the experimental data, while the red curve is their Gaussian fit. The abscissa of the peak value gives the offset o.

2023 JINST 18 P06027

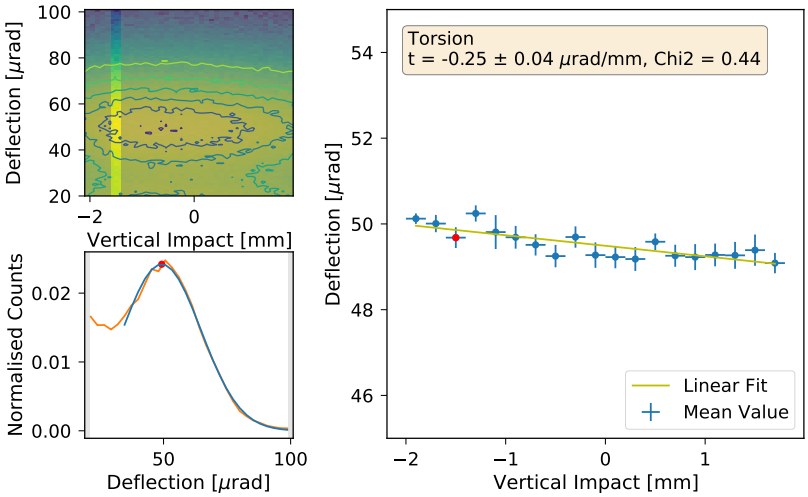

Figure 9. Example of torsion evaluation. Top left: density plot deflection vs vertical impact near the channeling deflection spot. Bottom left: deflection distribution (orange) and Gaussian fit (blue). Right: mean deflection values (blue circles) as a function of the vertical impact; a linear fit (green line) is used to evaluate the torsion. The slice considered for the example is highlighted in the top left plot and the mean value of the distribution is highlighted in red.

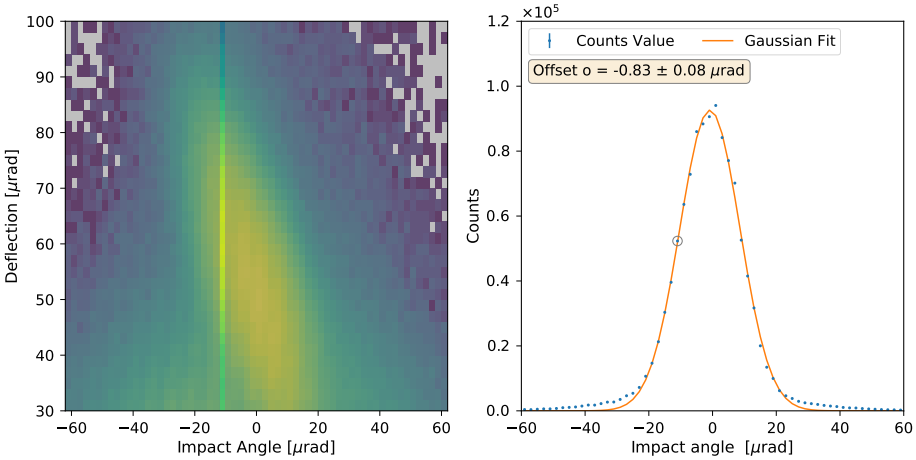

Figure 10. Example of offset evaluation. Left: density plot deflection vs impact angle near the channeling deflection. Right: count values for each slice (blue) and gaussian fit of the distribution (orange) as a function of the impact angle. The slice considered for the example is highlighted in the right plot and the counts are highlighted by the gray circle.

4.2.5 Mean value of the amorphous deflection

The deflection distribution in amorphous orientation might not be centred around zero. This behaviour is observed when the reference axis of the telescope is not perfectly aligned with that of the goniometer. The misalignment, often of few μrad, might also introduce a non negligible error in the evaluation of the bending angle, described in paragraph 4.2.6. A way to compensate the error consists in computing the mean value of the amorphous deflection and in subtracting it from the overall deflection distribution.

2023 JINST 18 P06027

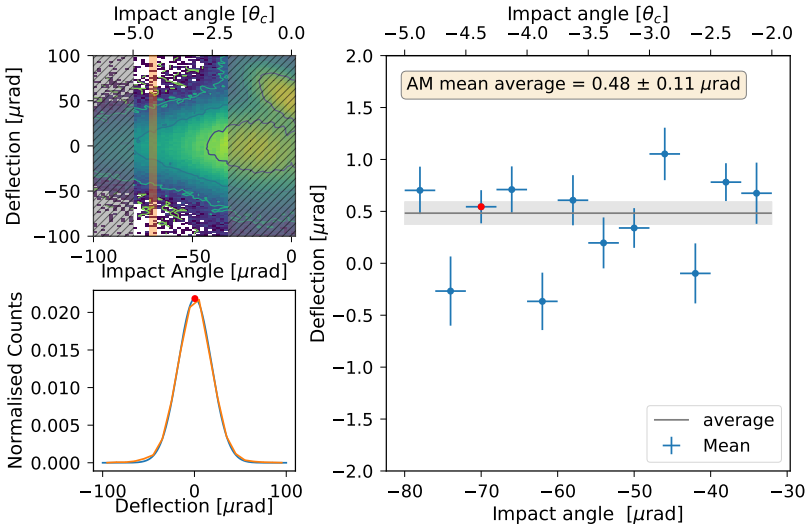

Figure 11. Example of amorphous (AM) deflection evaluation. Top left: density plot deflection vs impact angle, with the AM region highlighted; bottom left: deflection distribution (orange) and gaussian fit (blue). Right: mean deflection values (blue circles) as a function of the impact angle; a constant fit (grey line) is used to evaluate the AM mean value average. The slice considered for the example is highlighted in orange shade in the top left plot; the mean value of the distribution is highlighted in red.

In the example of figure 11, the events producing amorphous deflections are extracted from the data of a high-statistics angular scan. Having corrected the torsion and the offset of the deflection distribution using the equation (4.1), the angular range $\theta^{\mathbf{in}}_{\mathbf{corr}} \in [-5\theta_\mathbf{c}, -2\theta_\mathbf{c}]$, which includes only incoming particles in amorphous orientation, is segmented in slices of $0.5\,\theta_\mathbf{c}$ (top-left plot). The average value of the deflection is computed in each slice by a Gaussian fit (bottom-left plot). The histogram of the various slices is interpolated by a horizontal straight line (right plot). The mean value of the amorphous deflection θ_{AM} is given by the coefficient of the linear fit.

4.2.6 Channeling angle

The density plot of the horizontal deflection on the impact angle, corrected by torsion, offset and amorphous mean deflection, gives all the information needed for the crystal characterisation. It allows to select the angular regions of interest to produce the amorphous, the volume reflection and the channeling distributions. This is given by the shift from the horizontal axis of the mean value of the Gaussian distribution near the channeling spot. A two-dimensional Gaussian fit applied to the particles in the channeling spot is used to retrieve the mean values in both deflection and impact angle distributions. The former value gives the channeling bending (or deflection) angle, as shown in figure 12. The latter value, instead, is close with zero, because of the torsion and offset adjustment. Parameters of the 2D Gaussian fit, retrieved by the analysis script, are shown in the insert of figure 12.

2023 JINST 18 P06027

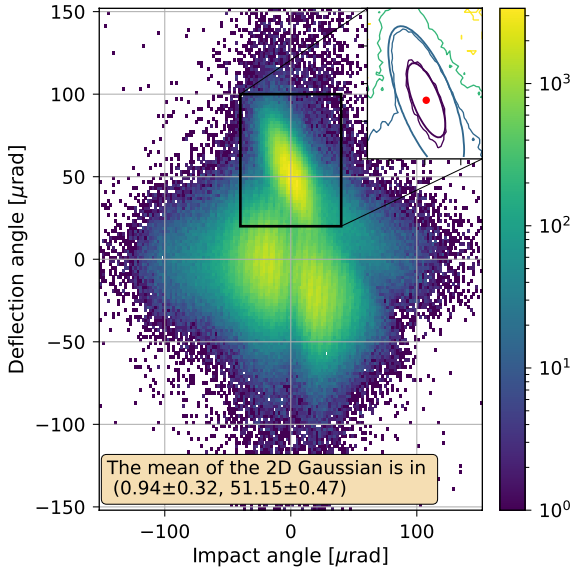

Figure 12. Density plot for the correlation between deflection and impact angle. In the magnified section on top right, the 2D Gaussian fit is applied to find the channeling deflection angle (red circle).

4.2.7 Channeling efficiency

The single-pass channeling efficiency is defined as the ratio of the particle flux in channeling states to the total flux inside the channeling acceptance. Such a parameter gives important information about the crystal quality, a fundamental assessment before installation in a circular accelerator. Its value is highly influenced by the angular distribution of the incident beam. During H8 tests, primary proton beams of 400 GeV energy have an angular divergence $\sigma(\theta_{\mathbf{x}}^{\mathbf{in}}) \approx 85$ µrad, generally smaller than the critical angle $\theta_{\mathbf{c}} = 10.6$ µrad, while for secondary hadron beams of 180 GeV energy the beam divergence is $\sigma(\theta_{\mathbf{x}}^{\mathbf{in}}) \approx 29$ µrad and the critical angle $\theta_{\mathbf{c}} = 16$ µrad.

Particles with an impact angle larger than $\theta_{\mathbf{c}}$ should be discarded to avoid underestimating the channeling efficiency. Two selection criteria are used: a more stringent, in which only particles with $|\theta_{\mathbf{x}}^{\mathbf{in}}| \leq \theta_{\mathbf{c}}/2$ are selected and another in which the full acceptance criterion $|\theta_{\mathbf{x}}^{\mathbf{in}}| \leq \theta_{\mathbf{c}}$ is applied. They provide information on how differently the core and the tails of the beam divergence contribute to the channeling process. An example of this is shown in figure 13. Superimposed on a density plot of the deflection versus the impact angles, the two shaded vertical bands encircle the two ensembles of incoming particles to be considered.

The two ensembles of particles produce the deflection distributions of figure 14, used to estimate the channeling efficiency as the ratio between the channeled to the total number of particles in each selection range. Between the amorphous and the channeling Gaussian peak several effects are present: mainly dechanneling, a few residuals from volume reflection and volume capture. To minimise contamination in counting the channeled particles, this value is estimated as twice the integral of the channeling half-peak, highlighted in figure 14. In conclusion, the channeling efficiency is evaluated as:

$$\eta_{\theta_{\mathrm{sel}}} = \frac{2 \times N_{\mathbf{CH}}[\mu_{\mathbf{CH}}, \mu_{\mathbf{CH}} + 3 \times \sigma_{\mathbf{CH}}]}{N_{\theta_{\mathbf{sel}}}}, \tag{4.3}$$

2023 JINST 18 P06027

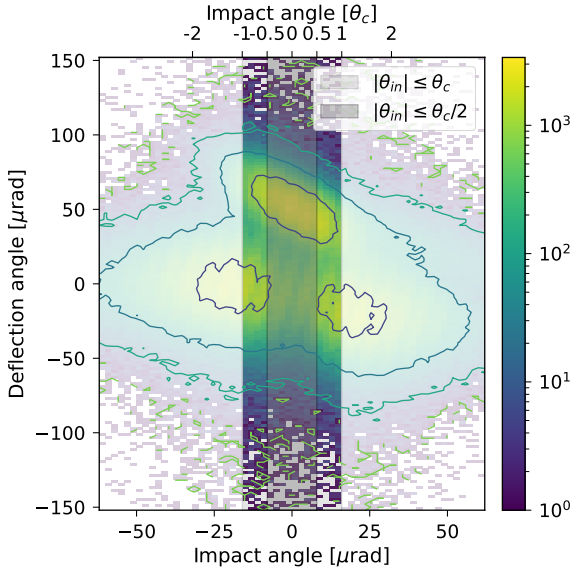

Figure 13. Density plot for the correlation between deflection and impact angle. The shades of grey highlight the impact angle selection for one (lighter) and half critical angle (darker) used to obtain the deflection distributions shown in figure 14.

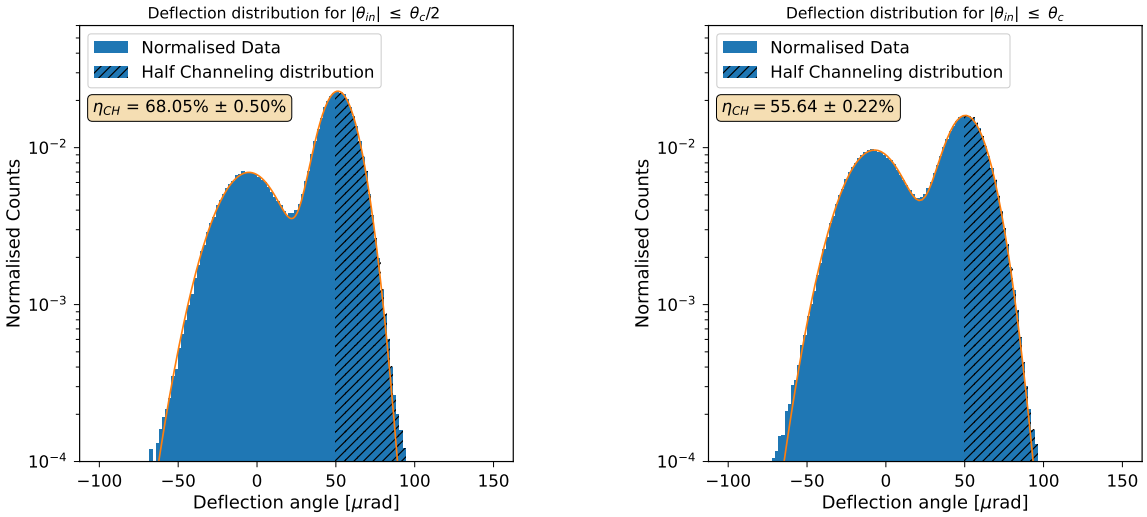

Figure 14. Deflection distributions for $|\theta_{\mathbf{x}}^{\mathbf{in}}| \leq \theta_{\mathbf{c}}/2$ (left) and $|\theta_{\mathbf{x}}^{\mathbf{in}}| \leq \theta_{\mathbf{c}}$ (right) (see figure 13). The hashed areas highlight the right side of the channeling Gaussian distribution used to integrate the total number of channeled particles.

where $\mu_{\mathbf{CH}}$ and $\sigma_{\mathbf{CH}}$ are the first and the second moments of the Gaussian channeling half-peak highlighted in figure 14, $N_{\mathbf{CH}}$ is the number of channeled particles in the same areas and $N_{\theta_{\mathbf{sel}}}$ is the total number of particles incident in the angular range $\theta_{\mathbf{sel}}$, corresponding to full or half acceptance for channeling.

2023 JINST 18 P06027

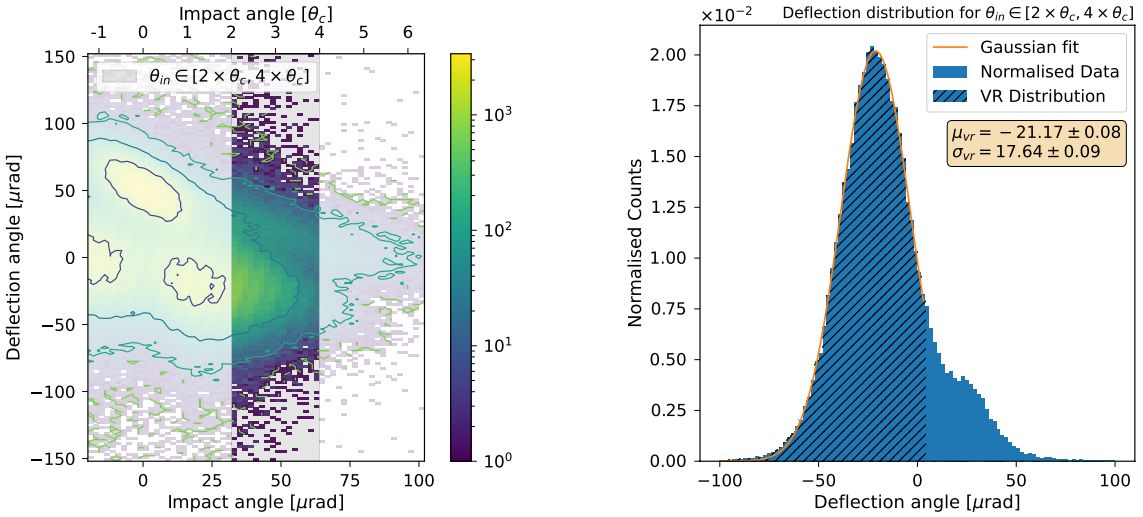

Figure 15. Example for volume reflection deflection evaluation. Left: density plot near the volume reflection region for deflection vs impact angle; the shades highlight the impact angle selection used to obtain the volume reflection deflection distribution. Right: deflection distribution (blue) and Gaussian fit (orange) used to obtain information on the $\theta_{\mathbf{VR}}$ angle.

The statistical error of the channeling efficiency is mainly related to the uncertainty of the integration limits in evaluating $N_{\mathbf{CH}}$. Assuming that the statistical errors of the first and second moments of the channeling distribution are $\delta\mu_{\mathbf{CH}}$ and $\delta\sigma_{\mathbf{CH}}$, respectively, the number of channeled particles varies between $N^{-}_{\mathbf{CH}}$ and $N^{+}_{\mathbf{CH}}$, defined as:

$$N^{\pm}_{\mathbf{CH}} = N_{\mathbf{CH}}[\mu_{\mathbf{CH}} \pm \delta\mu_{\mathbf{CH}}, \mu_{\mathbf{CH}} \pm \delta\mu_{\mathbf{CH}} + 3 \times (\sigma_{\mathbf{CH}} \mp \delta\sigma_{\mathbf{CH}}]. \tag{4.4}$$

where either the upper or lower notations should be considered, respectively. Using $N^{-}_{\mathbf{CH}}$ and $N^{+}_{\mathbf{CH}}$ in the eq. (4.3) the maximum overestimation and minimum underestimation of $\eta_{\theta_{\mathrm{sel}}}$ (at 66 % confidence level) is obtained. The half-difference between the minimum and maximum value of the efficiencies is considered as the efficiency error.

4.2.8 VR deflection angle

As for the channeling efficiency, the VR deflection can only be measured during tests with beams. The Volume Reflection deflection angle is independent of crystal characteristics, and for the beam energies used in the H8 tests, it is expected that $\theta_{\mathbf{VR}} \approx 1.3 \times \theta_{\mathbf{c}} \approx 21$ µrad [6].

In the data analysis, Volume Reflection is observed beside the channeling orientation over an angular range as wide as the crystal bending angle. An example is shown in figure 15. In the left plot the shaded angular range is the one where VR is predominant and coexists with a much smaller intensity of volume captured particles. The deflection $\theta_{\mathbf{VR}}$ is evaluated as the mean value of the compensated angular distribution over the incoming angular range $\theta^{\mathbf{in}}_{\mathbf{corr}} \in [2\theta_{\mathbf{c}}, 4\theta_{\mathbf{c}}]$. In the right plot, the deflection distribution is shown and a Gaussian fit is applied to identify the VR peak visible on negative deflection angles.

2023 JINST 18 P06027

5 Conclusions

The data analysis method presented has been developed to be self-consistent and to avoid as much as possible users arbitrary choices. Any data selection, handling or fitting is only based on the known description of the physics behind the observed process, and the working principle of the experimental apparatus. The full method as already been used by the UA9 collaboration to provide the CERN community insights on the performance of crystals before the installation in their accelerators.

Acknowledgments

The authors want to thank the UA9 collaboration for the access to the data, and hope that the method developed would be useful for future detailed measurements. Imperial College gratefully acknowledges financial support from the UK Science and Technology Facilities Council.

References

[1] J. Lindhard, *Influence of crystal lattice on motion of energetic charged particles*, *Kongel. Dan. Vidensk. Selsk., Mat. -Fys. Medd.* **34** (1965).

[2] E. Tsyganov, *Some aspects of the mechanism of a charge particle penetration through a monocrystal*, Fermilab TM-682, Batavia, Illinois 60520, U.S.A. (1976) [https://lss.fnal.gov/archive/test-tm/0000/fermilab-tm-0682.pdf].

[3] A.M. Taratin, *Particle channeling in a bent crystal*, *Phys. Part. Nucl.* **29** (1998) 437.

[4] A.M. Taratin and S.A. Vorobiev, *"Volume reflection" of high-energy charged particles in quasi-channeling states in bent crystals*, *Phys. Lett. A* **119** (1987) 425.

[5] W. Scandale et al., *Observation of nuclear dechanneling for high-energy protons in crystals*, *Phys. Lett. B* **680** (2009) 129.

[6] A.M. Taratin and W. Scandale, *Volume reflection of high-energy protons in short bent crystals*, *Nucl. Instrum. Meth. B* **262** (2007) 340.

[7] W. Scandale et al., *Volume reflection dependence of 400 GeV/c protons on the bent crystal curvature*, *Phys. Rev. Lett.* **101** (2008) 234801.

[8] W. Scandale et al., *High-efficiency volume reflection of an ultrarelativistic proton beam with a bent silicon crystal*, *Phys. Rev. Lett.* **98** (2007) 154801.

[9] W. Scandale, *Use of crystals for beam deflection in particle accelerators*, *Mod. Phys. Lett. A* **27** (2012) 1230007.

[10] A.G. Afonin et al., *First results of experiments on high-efficiency single-crystal extraction of protons from the U-70 accelerator*, *JETP Lett.* **67** (1998) 781.

[11] Y.M. Ivanov, A.A. Petrunin and V.V. Skorobogatov, *Observation of the elastic quasi-mosaicity effect in bent silicon single crystals*, *JETP Lett.* **81** (2005) 99.

[12] M. Pesaresi et al., *Design and performance of a high rate, high angular resolution beam telescope used for crystal channeling studies*, 2011 *JINST* **6** P04006.

[13] G. Hall et al., *A high angular resolution silicon microstrip telescope for crystal channeling studies*, *Nucl. Instrum. Meth. A* **924** (2019) 394.

2023 JINST 18 P06027

[14] G. Hall, T. James and M. Pesaresi, *Optimisation of a silicon microstrip telescope for UA9 crystal channeling studies*, 2020 *JINST* **15** C05014.

[15] W. Scandale et al., *Deflection of high energy protons by multiple volume reflections in a modified multi-strip silicon deflector*, *Nucl. Instrum. Meth. B* **338** (2014) 108.

[16] R. Rossi et al., *Track reconstruction of particle interactions in long crystals with large bending*, 2021 *JINST* **16** P05017.

[17] R. Rossi et al., *Measurements of coherent interactions of 400 GeV protons in silicon bent crystals*, *Nucl. Instrum. Meth. B* **355** (2015) 369.

[18] W. Scandale et al., *Angular asymmetry of the nuclear interaction probability of high energy particles in short bent crystals*, *Eur. Phys. J. C* **80** (2020) 27.

2023 JINST 18 P06027